# Accepted Manuscript


Transferring results from NIR-hyperspectral to NIR-multispectral imaging systems: A filter-based simulation applied to the classification of Arabica and Robusta green coffee

Rosalba Calvini, Jose Manuel Amigo, Alessandro Ulrici

PII: S0003-2670(17)30289-1

DOI: 10.1016/j.aca.2017.03.011

Reference: ACA 235112

To appear in: *Analytica Chimica Acta*

Received Date: 4 October 2016

Revised Date: 2 March 2017

Accepted Date: 6 March 2017

Please cite this article as: R. Calvini, J.M. Amigo, A. Ulrici, Transferring results from NIR-hyperspectral to NIR-multispectral imaging systems: A filter-based simulation applied to the classification of Arabica and Robusta green coffee, *Analytica Chimica Acta* (2017), doi: 10.1016/j.aca.2017.03.011.

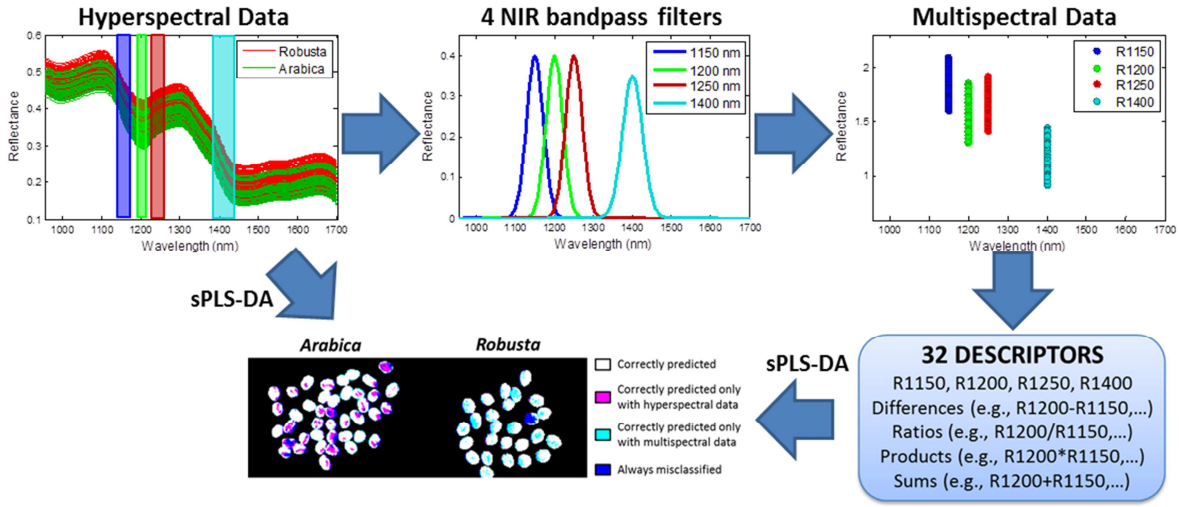

# Transferring results from NIR-hyperspectral to NIR-multispectral imaging systems: a filter-based simulation applied to the classification of Arabica and Robusta green coffee

Rosalba Calvini [a,*], Jose Manuel Amigo [b], Alessandro Ulrici [a]

[a] *Department of Life Sciences, University of Modena and Reggio Emilia, Padiglione Besta, Via Amendola 2, 42122 Reggio Emilia, Italy*

[b] *Department of Food Science, Faculty of Sciences, University of Copenhagen, Rolighedsvej 30, DK-1958 Frederiksberg C, Denmark*

* Corresponding author: Rosalba Calvini, Department of Life Sciences, University of Modena and Reggio Emilia, Padiglione Besta, Via Amendola 2, 42122 Reggio Emilia, Italy. Tel: +39 0522 5222048. Fax: +39 0522 522027. E-mail: rosalba.calvini@unimore.it.

**ABSTRACT**

Due to the differences in terms of both price and quality, the availability of effective instrumentation to discriminate between Arabica and Robusta coffee is extremely important. To this aim, the use of multispectral imaging systems could provide reliable and accurate real-time monitoring at relatively low costs. However, in practice the implementation of multispectral imaging systems is not straightforward: the present work investigates this issue, starting from the outcome of variable selection performed using a hyperspectral system. Multispectral data were simulated considering four commercially available filters matching the selected spectral regions, and used to calculate multivariate classification models with Partial Least Squares-Discriminant Analysis (PLS-DA) and sparse PLS-DA. Proper strategies for the definition of the training set and

the selection of the most effective combinations of spectral channels led to satisfactory classification performances (100% classification efficiency in prediction of the test set).

**KEYWORDS**

Green coffee; Multivariate classification; Hyperspectral imaging; Multispectral imaging; Sparse methods.

## 1. INTRODUCTION

Hyperspectral imaging (HSI) systems have showed a great potential for their application in food control processes, being a fast and non-destructive technique able to handle different issues related to quality evaluation and safety inspection of agricultural and food products [1 – 3]. The main advantage of HSI is the possibility of coupling classical point-wise spectroscopy with imaging techniques, in order to obtain simultaneously spatial and spectral information from a sample. In this manner, a huge amount of spectral information is achieved from the surface of a sample in a relatively short time and it is possible to provide a reliable and accurate real-time monitoring at different stages of the food processing chain [4].

Despite the advantages of this technique, two main drawbacks currently limit the direct implementation of HSI into real-time systems for food control: the high costs of HSI systems and the extremely large amount of data that are acquired in short times, implying high computational loads which complicate the development of efficient and fast applications [5, 6]. For these reasons, most of the food related HSI research works have been directed towards the identification of wavelengths relevant to the problem at hand, for further development of multispectral imaging systems suitable for on line or portable devices [3, 4, 7]. The advantages of multispectral imaging systems over hyperspectral ones include the faster acquisition times and the lower costs of hyperspectral cameras [8]. Furthermore, multispectral technology is easier to implement for on-line applications, due to the higher resistance and stability of the optical components.

Starting from variable selection performed on hyperspectral image data, a multispectral imaging system can be implemented, at least in principle, by using the selected spectral regions [9 – 12]. However, adapting the outcomes of variable selection performed on hyperspectral data to a filter-based imaging system is not straightforward, and it is not easy to maintain acceptable performances after transferring results from a hyperspectral imaging system to a multispectral imaging one [10]. In fact, position and width of actually available filters generally do not perfectly match the selected

spectral regions. Moreover, in multispectral systems only a single "average" intensity value can be measured for each selected spectral region, which implies that the useful information related to spectral shape within the selected intervals is lost. On the other hand, the limited number of multispectral channels allows to easily expand the number of potentially useful descriptors by calculating quantities derived from the single channel intensities, i.e., by introducing nonlinear and interaction terms derived from the intensity values in order to improve the results [13]. In this manner, it is possible to evaluate linear and non-linear relationships between the different channels and thus to emphasize small variations in the spectral signature which could be useful for the problem at hand [14].

In this context, the present work is aimed at showing the feasibility of implementing a simulated multispectral filter-based classification model for the discrimination of green coffee samples belonging to Arabica (*Coffea arabica*) and Robusta (*Coffea canephora*) coffee species. Arabica and Robusta coffee differ each other from chemical and organoleptic properties. Chemical analysis based on chromatography showed that Arabica and Robusta coffee have differences in their content in caffeine, cholorogenic acid, trigonelline, sterols and amino acids [15, 16]. Furthermore, Arabica coffee is considered of higher quality because of its better taste and aroma and, therefore, it is generally preferred by the consumers. On the other hand, Arabica coffee can be two to ten times more expensive than Robusta coffee, which is less appreciated and mainly used as filler in coffee blends or in instant coffee production [17, 18]. Due to the significant differences in terms of both price and quality, it is therefore important to correctly discriminate between the two coffee coffee species in order to prevent the adulteration of high quality Arabica coffee with cheaper and lower quality Robusta coffee [19 - 22]. Therefore, the correct classification of green coffee beans of the two species could allow to identify possible adulterations or mislabelling at an early stage of the processing chain.

Many different analytical techniques have been investigated in order to discriminate Arabica and Robusta coffee species, including $^{1}$H-Nuclear Magnetic Resonance (NMR) [23], $^{13}$C-NMR [24], 2-

D electrophoresis [25], electronic nose and electronic tongue [26] among others. The use of so many different analytical methods suggest that a reliable discrimination between Arabica and Robusta species is a crucial aspect for coffee industry.

However, the above mentioned methods are not suitable for fast characterization of large amounts of products, e.g., by rapid in-line or on-line monitoring [19]; conversely, spectroscopic methods represent a fast and non-destructive alternative to other more complex analytical techniques for facing food authentication problems, being at the same time simple, fast, non-destructive and reliable [27]. In particular, classical point-wise NIR spectroscopy has been widely used to discriminate Arabica and Robusta species, both on green coffee [28, 29] and on roasted coffee [30, 31]. More recently, some research works have been also reported where hyperspectral imaging (HSI) is used to characterize these coffee species [32, 33].

The main aim of the present study is to investigate the issues related to the implementation of a multispectral imaging system starting from the outcome of a variable selection/classification model calculated on hyperspectral data [7]. In particular, a multispectral detection system was simulated by considering four commercially available filters, chosen as those showing the best match with the selected spectral regions. Then, Partial Least Squares Discriminant Analysis (PLS-DA) [6, 34, 35] classification models were built considering as descriptors both the four channels alone and the four channels together with their squared values and sums, differences, products and ratios between couples of channels. Moreover, variable selection by Sparse Partial Least Squares Discriminant Analysis (sPLS-DA) [7, 36] was also employed in order to identify the most relevant descriptors and to further increase the performances of the classification models.

## 2. MATERIALS AND METHODS

### 2.1 Coffee samples

The green coffee samples of Arabica and Robusta species considered in this study came from different geographical areas and were provided by a local roasting company during a period of 6 months. In particular, each sample belonged to a different batch and the samples were subjected to different processing methods to separate the seed form the fruit. Despite the different properties of the samples, we focused on the discrimination between Arabica and Robusta coffee species, regardless of processing method or of geographical origin.

On the whole, 33 batches were considered in the industrial plant: 18 of Robusta and 15 of Arabica. From each batch about 500 g of beans, sampled in order to be as representative as possible of the corresponding batch, were collected and stored in a sealed package. From each package, three aliquots of 70 g of randomly selected beans were taken, and for each aliquot two repeated images were acquired, shuffling the beans between the two acquisitions. The same procedure was repeated in a different day in order to check the day-to-day variability. All the batches were acquired in random order and the packages were sealed again and stored at room temperature between the different acquisition days. Therefore, for each batch 12 hyperspectral images (= 2 measurement sessions × 3 aliquots × 2 repeated acquisitions) were acquired, obtaining a dataset composed by 396 hyperspectral images (33 batches × 12 images).

### 2.2 Image acquisition

The hyperspectral images were acquired using a desktop NIR Spectral Scanner (DV Optic) embedding a reflectance imaging based spectrometer Specim N17E, coupled to a Xenics XEVA 2608 camera (320 × 256 pixels) and working in the 955-1700 nm spectral range with a spectral resolution of 5 nm, with a total of 150 spectral channels. The images were acquired using a black silicon carbide sandpaper sheet as background, which is characterized by a very low and constant

reflectance spectrum [37], and in addition a 99% white ceramic tile reflectance standard and two ceramic tiles with intermediate reflectance values were included in the area of the images.

The raw data were converted into reflectance values using an instrumental calibration based on the high reflectance standard reference and on dark current [38]. Furthermore, in order to reduce the variability among images over time, an additional internal calibration was performed [6, 39], based on the average reflectance values of the reflectance standard, of the two ceramic tiles and of the black silicon carbide sandpaper.

Before further analysis, the pixels related to the black sandpaper background were removed from each image using the following thresholding procedure: a preliminary evaluation of some sample images allowed to identify the most discriminant wavelength by maximizing the Fisher ratio between background spectra and sample spectra. In this manner, at 1050 nm, all the pixels below the threshold value of 0.1 reflectance units were identified as background and removed.

## 2.3 Data analysis

### *2.3.1 Data arrangement*

The acquired hyperspectral images were used to create different hyperspectral datasets, which in turn were converted into the corresponding multispectral datasets and then used for calculation and validation of the classification models.

In particular, the 33 coffee batches were randomly split in 24 training batches (corresponding to 288 training set images), including 11 Arabica and 13 Robusta coffee batches, and in 9 test batches (108 images), including 4 Arabica and 5 Robusta coffee batches.

Two different strategies were then considered for the definition of the training set:

- Average Spectra (AS): the average spectrum was calculated for each training set image, obtaining an AS training set including 288 spectra;
- Random spectra (RS): 50 spectra were randomly selected from each training set image, obtaining a RS training set including 14400 spectra (= 288 images × 50 spectra).

Since each hyperspectral image is composed by tens of thousands of single-pixel spectra, AS training set and RS training set represent two different approaches to build a reduced (but still representative) training set from the huge amount of data contained in the original images.

On one hand, computing the average spectra from each hyperspectral image allows to drastically reduce the number of objects, under the assumption that an average spectrum is representative of the image as a whole. On the other hand, averaging all the pixel-spectra contained in each image implies loosing the information about the spatial variability within each image. Therefore, keeping a relatively limited number of randomly selected spectra for each image was considered as a valid compromise between reducing data size and (at least partly) maintaining spatial variability related information.

The classification performances of the two approaches were evaluated in prediction both at the image-level, i.e., considering each image on the whole, and at the pixel-level, i.e., evaluating the class assignment of each single image pixel. In particular, an external test set consisting of the average spectra of each image of the test samples was used to validate the classification models at the image-level. Moreover, in order to validate the classification models also at the pixel-level and to visually evaluate the classification performances, two different test images (test image 1 and test image 2) with different arrangement of the beans were considered. The test images were obtained by merging together one image of Arabica coffee and one of Robusta coffee taken from the test samples. In this manner, since each test image contains one image for each class, it was possible to obtain a quantitative evaluation of the predictive ability of the models at the pixel-level.

The hyperspectral datasets (AS training set, RS training set, test set and the two test images) mentioned in this section were then converted into multispectral data following the procedure described in below.

*2.3.2 From HSI selected spectral regions to multispectral data*

Number and position of the channels to be considered for the multispectral system were defined on the basis of feature selection made by applying sparse classification methods to the AS training set described in the previous section, as reported in Calvini et al., 2015 [7]. Briefly, sparse methods allow performing variable selection by forcing the model coefficients related to noisy or uninformative variables to be equal to zero, in a way that it is possible to calculate a classification model and to perform variable selection in a one-step procedure [40]. For the classification of Arabica and Robusta green coffee two different sparse-based algorithms, i.e., sparse Principal Component Analysis [41] coupled with k-Nearest Neighbour [42] (sPCA+kNN) and sparse Partial Least Squares Discriminant Analysis (sPLS-DA) [36], were applied to the average spectra of the hyperspectral images. The relevance of the selected wavelengths, which are reported in Figure 1.a, was confirmed by the fact that both sparse classification methods converged to the selection of the same narrow spectral regions. The evaluation of these regions showed that they essentially reflect chemical composition differences between the two coffee varieties, rather than physical effects. In particular, the selected spectral regions were related to the C-H aromatic second overtone (1143 nm), to the C-H aliphatic second overtone (1195-1225 nm), and to the O-H first overtone of aliphatic (1410 nm) and aromatic alcohol (1420 nm) [43]. In order to better evaluate the spectral differences between Arabica and Robusta green coffee, Figure S-1 reports two sample spectra belonging to the two coffee species and the corresponding difference spectrum.

Starting from the outcome of variable selection performed on hyperspectral data, the commercial filters showing the best match with the selected spectral regions were then identified [44]; in particular, four bandpass filters were selected, whose center wavelength (*CWL*), filter width at half maximum (*FWHM*) and peak transmission (*PT*) values listed below:

- Filter 1: CWL=1150 nm, FWHM=10 nm, PT=40%
- Filter 2: CWL=1200 nm, FWHM=10 nm, PT=40%
- Filter 3: CWL=1250 nm, FWHM=10 nm, PT=40%

- Filter 4: CWL=1400 nm, FWHM=12 nm, PT=35%.

In order to mimic the output of a filter-based multispectral system, each reflectance spectrum of the hyperspectral datasets (AS training set, RS training set, test set and the two test images) was then used to estimate the reflectance values that would be obtained by using the considered filters.

To this purpose, the Gaussian-shaped transmission profile of each filter was calculated from the corresponding filter properties as:

$$Z(\lambda) = PT \frac{1}{\sigma\sqrt{2\pi}} e^{-\frac{(\lambda - CWL)^2}{2\sigma^2}} \quad (1)$$

where Z($\lambda$) is the Gaussian transmission profile of the filter as a function of the wavelength $\lambda$, and σ is the standard deviation of the Gaussian distribution, which is related to *FWHM* according to the equation [45]:

$$\sigma = \frac{FWHM}{2\sqrt{2\ln 2}} \quad (2)$$

For each filter, the corresponding reflectance value of each object *i* belonging to the hyperspectral datasets was then calculated according to the equation:

$$R_i = \sum_{\lambda_{min}}^{\lambda_{max}} Z(\lambda)\, S_i(\lambda) \quad (3)$$

where $S_i(\lambda)$ is the HSI spectrum of object *i*, while $\lambda_{min}$ and $\lambda_{max}$ are the extreme values of the spectral rage acquired with the hyperspectral camera (in our case, $\lambda_{min}$ = 955 nm and $\lambda_{max}$ = 1700 nm).

This procedure is schematically represented in Figure 1, where Figure 1.a reports the spectra of AS training set together with the selected spectral regions, Figure 1.b shows the Gaussian profiles calculated by equation (1), and Figure 1.c reports the 4 discrete reflectance values calculated by equation (3) for each spectrum of the AS training set.

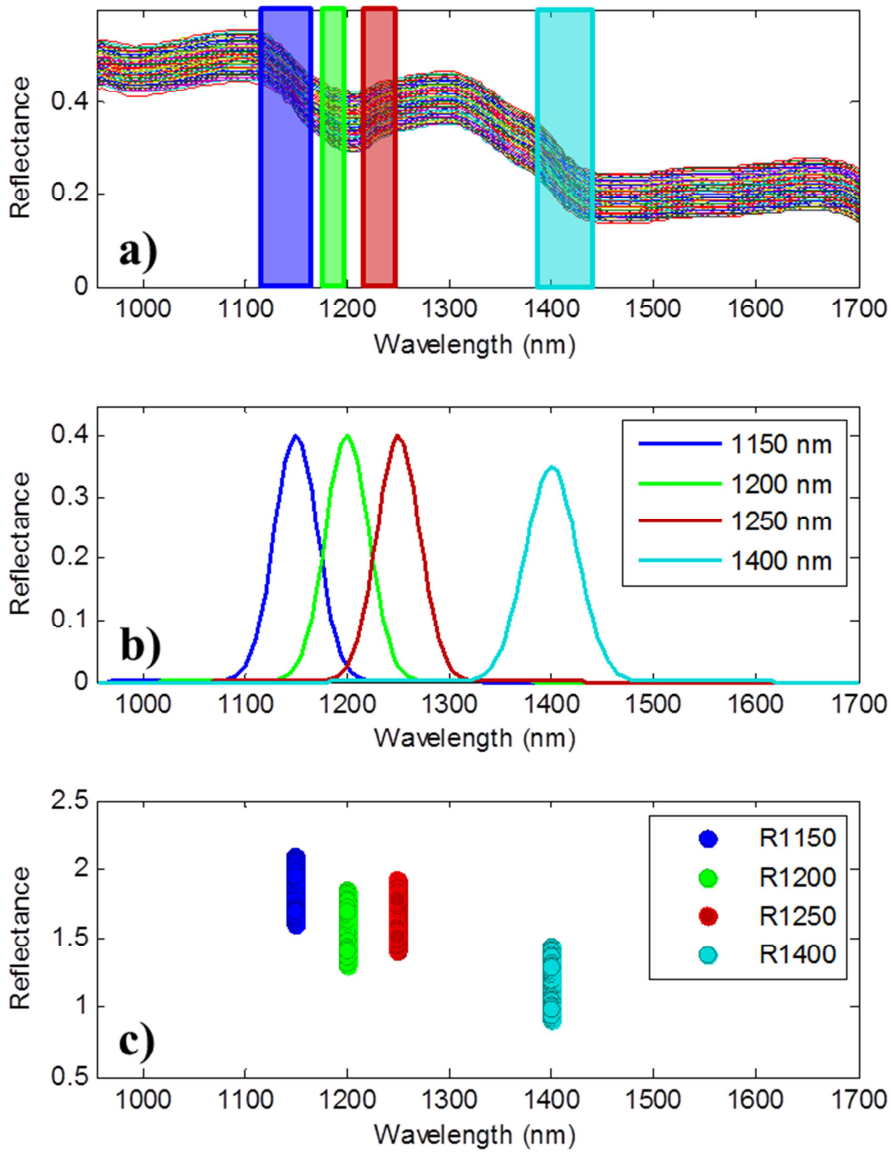


**Figure 1.** Average spectra calculated from each image of the training samples with selected regions highlighted (a), Gaussian profiles of the 4 considered filters (b) and resulting reflectance values obtained from the average training spectra (c).

Therefore, from the original hyperspectral datasets containing 150 spectral variables, the corresponding multispectral datasets containing 4 variables were obtained, where each variable is the reflectance value of a given multispectral channel. As an example, Figure S-2 (Supplementary material) shows the pseudocolor images obtained from the four considered channels for both test image 1 and test image 2.

*2.3.3 Filter-based simulations*

Starting from the multispectral datasets composed of 4 variables, three different simulations were performed:

- In *Filter Simulation 1* only the 4 reflectance values of the filters were considered for PLS-DA classification.
- In *Filter Simulation 2*, since the low number of multispectral channels allows expanding the number of potentially useful descriptors by calculating quantities derived from the outputs of the different channels, PLS-DA classification models were calculated including also additional descriptors derived from the four reflectance values. In particular, the squared reflectance value of each channel and differences, ratios, products and sums between couples of channels were calculated, obtaining datasets with the 32 descriptors listed in Table 1.
- In *Filter Simulation 3*, feature selection by sPLS-DA was performed in order to identify the most relevant descriptors among the 32 variables listed in Table 1.

For each of the three simulations, two classification models were calculated, one using the AS training set and one using the RS training set.

| Single Filters | Differences | Ratios | Products | Sums |
|---|---|---|---|---|
| R1150 | R1200-R1150 | R1150/R1200 | R1150*R1200 | R1150+R1200 |
| R1200 | R1250-R1200 | R1150/R1250 | R1150*R1250 | R1150+R1250 |
| R1250 | R1400-R1250 | R1150/R1400 | R1150*R1400 | R1150*R1400 |
| R1400 | R1400-R1200 | R1200/R1250 | R1200*R1250 | R1200+R1250 |
| $R1150^2$ | R1400-R1150 | R1200/R1400 | R1200*R1400 | R1200+R1400 |
| $R1200^2$ | R1250-R1150 | R1250/R1400 | R1250*R1400 | R1250+R1400 |
| $R1250^2$ | | | | |
| $R1400^2$ | | | | |

**Table 1.** List of the 32 descriptors considered.

*2.3.4 PLS-DA and sPLS-DA*

PLS-DA [34] is a classification method based on the application of PLS regression to classification purposes. In PLS-DA the **Y** matrix is composed by as many columns as the number of existing classes, where each column is a binary class vector, reporting the 1 value if the corresponding row (object) belongs to the class, and 0 otherwise. The matrix of descriptors (**X**) is therefore regressed against the **Y** binary matrix, and the outcome of the PLS model is a matrix containing the regression coefficients which are used to predict new samples. The Y predictions for each object with respect to each class are continuous values, therefore a threshold based on Bayesian statistics [46] has to be set separately for each class model (i.e. for the estimate of each class vector), so that objects whose predicted value for a given class is higher than the threshold are attributed to that class, while objects leading to predictions lower than the threshold are not assigned to the class.

Sparse PLS-DA [7, 36] is an extension of PLS-DA in which a penalty function is applied to the model parameters in order to constrain some coefficients to be equal to zero, i.e., to induce sparsity on the model coefficients. In particular, sparsity is induced on the PLS loadings, and consequently on the regression coefficients used to predict unknown samples. Therefore, thanks to the sPLS-DA approach it is possible to perform both classification and variable selection in a one-step procedure, by forcing to zero the coefficients of noisy or uninformative variables.

In order to select the best sPLS-DA classification models, in addition to the number of latent variables (LVs) like for PLS-DA, also the number of variables to select for each component needs to be tuned. Therefore, in Filter Simulation 3, different sPLS-DA models were constructed using both AS training set and RS training set, and testing all the combinations between a number of LVs ranging from 1 to 5 and a number of variables to select for each component ranging from 2 to 32. For each training set, the best model was selected by keeping the classification error in cross-validation as low as possible, while retaining at the same time the lowest possible number of variables and of LVs.

Both PLS-DA and sPLS-DA were calculated on autoscaled variables since the considered descriptors have different scales. The optimization of the classification models was performed using contiguous blocks cross-validation with 4 deletion groups, where each block contained the average spectra (for AS training set) or randomly selected spectra (for RS training set) of all the replicated and repeated images belonging to 6 batches (i.e., setting aside whole batches in the different deletion groups), as shown in Figure S-3 of Supplementary material.

For all the simulations, the classification performances were defined using efficiency (*EFF*), which is the geometric mean between sensitivity (*SENS*) and specificity (*SPEC*), i.e.:

$$EFF = \sqrt{SENS \times SPEC} \qquad (4)$$

where sensitivity is the percentage of objects of each class correctly retained by the class model and specificity is the percentage of objects of the other classes correctly rejected by the class model.

Data analysis was performed using PLS_Toolbox (v. 7.5, Eigenvector Research Inc., USA) for PLS-DA, while sPLS-DA was computed with *ad-hoc* routines kindly provided by Dr. Ewa Szymanska and written in Matlab language (ver. 7.12, The Mathworks Inc., USA); further details can be found in Szymanska et al., 2015 [47]. The data were analyzed using a personal computer running with Windows 8.1-64 bit and equipped with an Intel Core® i7-3632QM CPU @ 2.20GHz processor and 6.00 GB RAM.

# 3 RESULTS AND DISCUSSION

## 3.1 Filter Simulation 1

The results obtained from the PLS-DA classification models built both using AS training set and RS training set and considering only the reflectance values of the 4 channels are reported in the first two columns of Table 2. Concerning calibration and cross validation, the PLS-DA model built using AS training set gives definitely best results than the one built with RS training set. However, AS training set and RS training set show comparable results for the test set of average spectra and RS training set gives better results when used to predict both test images at the pixel level. These differences are likely due to the fact that the variability among spectra belonging to the same class is much higher in RS training set than in AS training set. On the one hand, this led to worst results of RS training set in calibration and cross validation, but on the other hand it turned out to be useful for the predictions of the test images at the pixel-level.

| | **Filter Simulation 1** | | **Filter Simulation 2** | | **Filter Simulation 3** | |
|---|---|---|---|---|---|---|
| | **AS tr. set** | **RS tr. set** | **AS tr. set** | **RS tr. set** | **AS tr. set** | **RS tr. set** |
| **N° variables** | 4 | 4 | 32 | 32 | 4 | 4 |
| **LVs** | 4 | 4 | 3 | 3 | 2 | 2 |
| $\boldsymbol{EFF_{CAL}}$ | 99.1 | 81.3 | 100.0 | 80.3 | 99.6 | 78.4 |
| $\boldsymbol{EFF_{CV}}$ | 97.3 | 79.9 | 99.3 | 78.7 | 97.3 | 78.0 |
| $\boldsymbol{EFF_{TEST}}$ | 94.0 | 94.9 | 97.5 | 100.0 | 98.3 | 100.0 |
| $\boldsymbol{EFF_{IMG1}}$ | 65.1 | 74.0 | 71.1 | 71.0 | 69.5 | 83.9 |
| $\boldsymbol{EFF_{IMG2}}$ | 83.9 | 92.2 | 84.3 | 92.1 | 85.6 | 93.1 |

**Table 2.** Results obtained using AS training set and RS training set in filters simulation1, filter simulation 2 and filter simulation 3; the classification efficiency values are referred to the results in calibration ($EFF_{CAL}$), cross-validation ($EFF_{CV}$), prediction of the test set at the image-level ($EFF_{TEST}$), and of test image 1 and test image 2 at the pixel-level ($EFF_{IMG1}$ and $EFF_{IMG2}$, respectively).

In fact, the predicted image obtained when AS training set was used to classify test image 1 (Figure 2.a), in which the pixels predicted as Arabica coffee are represented in red colour and the pixels

predicted as Robusta coffee are represented in green colour, shows that the classification performances are strongly influenced by the round shape of the beans. Actually, when dealing with the classification of objects using hyperspectral or multispectral imaging systems, the problem of the irregular shape of the samples is often present, since in practical applications the sample surface is not generally flat. This might be ascribed to a lower signal in the spectra or to the fact that the signal is mixed with the background signal.

The same model applied to test image 2 gives a higher *EFF* value, but the problem of the shape still occurs (Figure 2.b). In the case of the beans belonging to Robusta coffee (group of beans on the right) the misclassified pixels can be found mainly in correspondence of the edges of the beans. Furthermore, considering the beans belonging to Arabica coffee, some of those beans are misclassified (Figure 2.b).

Conversely, the shape effect is less evident when the same images are predicted with RS training set (Figures 2.c and 2.d). In particular, the results for test image 1 (Figure 2.c) show that one Robusta bean is clearly misclassified, and the same for some Arabica beans. Concerning test image 2, the major part of pixels is assigned to the correct class, even if some misclassifications occur at the edges of the beans (Figure 2.d). The differences in prediction on the test images of the two approaches are highlighted in Figure 2.e and Figure 2.f, which represent a difference image between the predictions made from AS training set and RS training set on the same image. In particular, the pixels correctly predicted with both approaches are represented in blue colour, the pixels misclassified with both approaches are represented in purple colour and those differently predicted (i.e., where only one of the two models have failed) are represented in yellow colour.

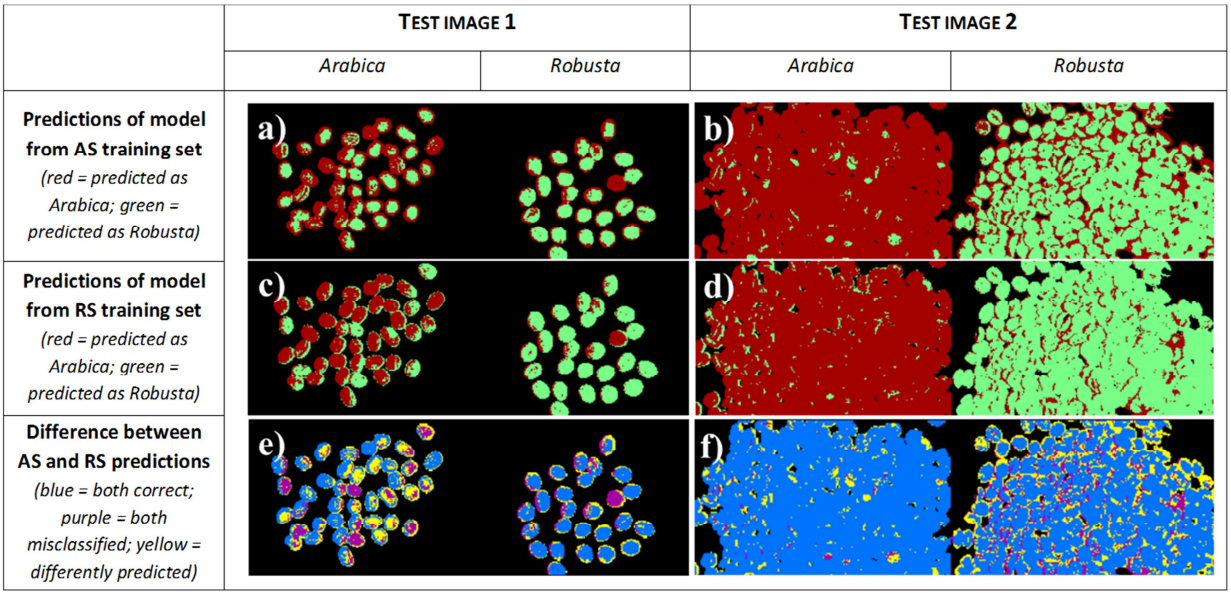


**Figure 2.** Filter simulation 1: predicted images of PLS-DA models built using AS training set (a, b) and RS training set (c, d), and difference images for test image 1 (e) and test image 2 (f).

Moreover, Table S-1 (Supplementary material) reports the percentage of correctly predicted pixels of Arabica and Robusta classes for both the test images. While the percentage of correctly predicted pixels for Arabica Coffee does not depend significantly upon the considered training set, the percentage of correctly predicted pixels for Robusta coffee is much higher when RS training set is used.

### 3.2 Filter Simulation 2

In Filter Simulation 2, the PLS-DA models were calculated using all the 32 descriptors listed in Table 1; the results obtained with the AS and the RS training sets are reported in the third and fourth column of Table 2, respectively. Interestingly, for both the AS and RS training sets only three LVs have been selected.

As observed in Filter Simulation 1, the classification model built using AS training set shows better performances in calibration and cross validation than the one built on RS training set. However, the model based on RS training set shows better results for the prediction both of test set and of test image 2. In particular, an *EFF* value equal to 100% is obtained when the classification model built

using RS training set is used to predict the test set. The performances in the prediction of test image 1 are essentially the same in terms of efficiency values, but AS training set gives a higher percentage of Arabica pixels which are correctly predicted (76.8%), while RS training set gives a higher percentage of correctly predicted pixels for Robusta class (86.0%).

Comparing the results obtained for Filter Simulation 2 with those of Filter Simulation 1, it can be observed that, for the models calculated using AS training set, the use of additional descriptors led to a general increase of the *EFF* values; conversely, for the models calculated using RS training set, Filter Simulation 2 led to slightly worse results, except for the prediction of the test set.

Concerning the pixel-level predictions, Figures S-4.a and S-4.b (Supplementary material) report the predictions obtained using AS training set for test image 1 and test image 2, respectively. In both the images the problem of the round shape of the beans is less evident than in the corresponding predicted images obtained from Filter Simulation 1, even if many misclassifications still occur in correspondence to the edges and to the centre cut of the beans. Moreover, also the percentage of pixels correctly predicted generally increases from Filter Simulation 1 to Filter Simulation 2 for both test images mainly considering class Arabica.

Concerning the model built using RS training set, Figures S-4.c and S-4.d (Supplementary material) report the predictions of test image 1 and test image 2, which look very similar to those obtained in Filter Simulation 1.

The corresponding regression vectors have been reported in Figures 3.a and 3.b, respectively. For both the classification models, single reflectance values, sums and products have low influence, since the absolute values of the corresponding regression coefficients are small. The largest absolute values of the regression coefficients are instead observed for some differences and ratios; in particular, R1250-1200 and R1200/R1250 are the descriptors showing the highest contribution for both the models. More in general, the two regression vectors are quite similar to each other, suggesting that - independently of the considered training set - the information useful to discriminate between Arabica and Robusta coffee is found within the same subset of descriptors.

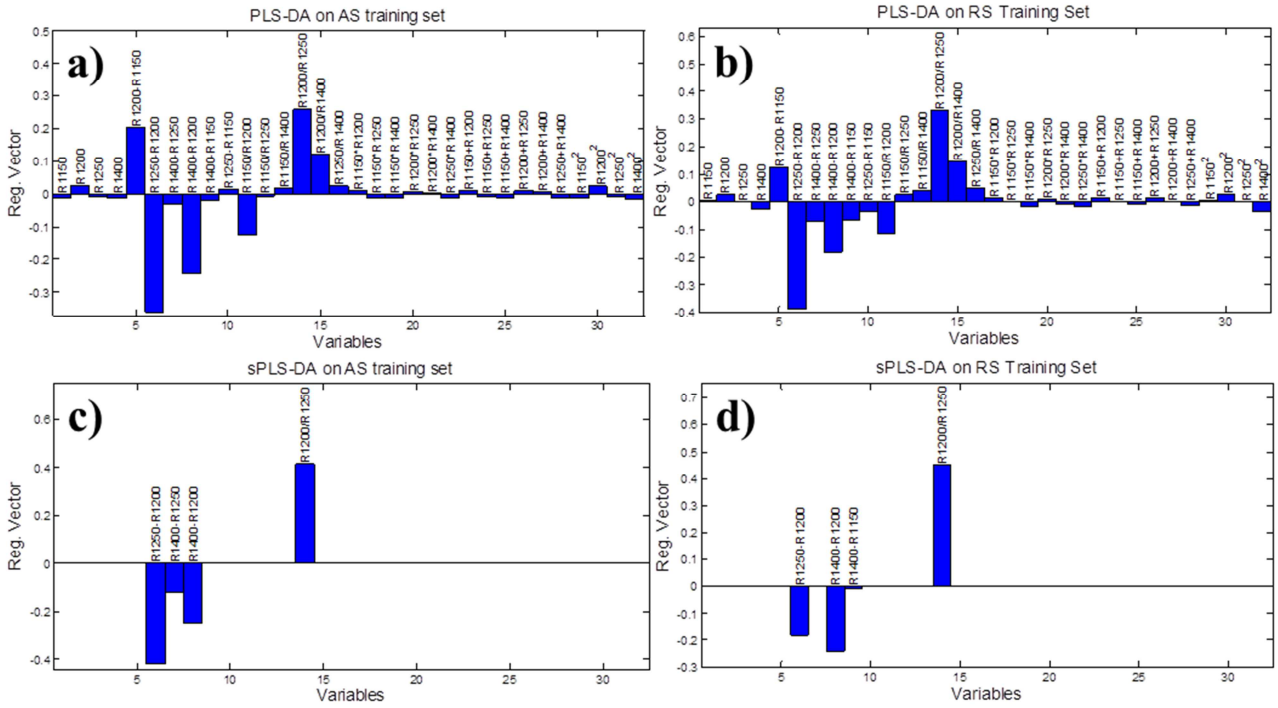


**Figure 3.** PLS-DA regression vectors of the classification models built on AS training set (a) and RS training set (b) considered in filter simulation 2; and regression vectors of sPLS-DA models calculated on AS training set (a) and RS training set (b) in filter simulation 3.

### 3.3 Filter Simulation 3

In order to better identify the most relevant descriptors involved in the discrimination between Arabica and Robusta coffee beans and to reduce the number of variables used in the classification models, feature selection by sPLS-DA was then applied both to AS and to RS training sets.

Figure S-5 (Supplementary material) reports the response surfaces for AS and for RS training sets (Figures S-5.a and S-5.b, respectively) of the *EFF* values estimated in cross-validation as a function of the number of LVs and of the number variables selected for each LV. In both the cases, the optimal conditions were reached with 2 LVs and 2 variables for each component, which correspond to regression vectors including 4 selected variables, as reported in Figure 3.c for AS training set and in Figure 3.d for RS training set. Both sparse models converge on the selection of the three descriptors showing the highest absolute values of the corresponding regression coefficients, i.e.,

R1250-R1200, R1400-R1200 and R1200/R1250; moreover, R1400-R1250 and R1400-R1150 are additionally selected in the sparse model built on AS training set and RS training set, respectively.

The results of the sparse models are reported in the last two columns of Table 2. Similarly to the results of Filter Simulations 1 and 2, also for Filter Simulation 3 the *EFF* values obtained in calibration and in cross-validation for RS training set are lower than those obtained for AS training set, while higher performances have been obtained in prediction, both at the image-level and at the pixel-level. In particular, the use of the RS training set led to an *EFF* value equal to 100% for the prediction of the test set at the image-level; the corresponding sLV1 and sLV2 score plot is reported in Figure S-6 (Supplementary material) which shows a distinct separation of the samples belonging to Arabica and Robusta coffee species.

In general, compared to the use of the 4 reflectance values of the filters (Filter Simulation 1), the selection by sPLS-DA of the most relevant descriptors allowed to obtain more parsimonious models (2 LVs instead of 4 LVs), and to gain a significant increase of the classification performances in prediction, in particular for the model calculated using the RS training set.

As far as the prediction at the pixel-level is concerned, the comparison of the predicted images obtained from AS training set (Figures 4.a and 4.b for test image 1 and test image 2, respectively) and from RS training set (Figures 4.c and 4.d for test image 1 and test image 2, respectively) shows that the sparse model built using AS training set is much more sensitive to the round shape of the coffee beans, this fact being particularly evident in the case of test image 1. Moreover, in the prediction of test image 1 for both models more misclassifications occur for Arabica coffee beans (on the left) than for Robusta coffee beans (on the right). Indeed, for both models the percentage of correctly classified Robusta coffee pixels is greater than the percentage of correctly classified Arabica coffee pixels (Table S-1 in Supplementary material).

As far as test image 2 is concerned, even if the overall classification of the beans is correct for both models, the sparse classification model built using RS training set is less sensitive to edge effects and to the round shape of the beans (Figure 4.d). This is also evident from the difference image

between the predictions made with AS training set and RS training set, reported in Figures 4.e and 4.f, respectively: considering test image 1, one Robusta bean and four Arabica beans are always misclassified (purple colour), while the pixels differently predicted (yellow colour) are mainly ascribable to the fact that the model built using AS training set is more influenced by the shape of the beans. Conversely, in test image 2 the overall classification of the beans is correct for both classes; also in this case the differences are mainly due to a higher sensitivity to shape-related effects in the model built using AS training set, as it is also confirmed by the values reported in Table S-1 (Supplementary material).

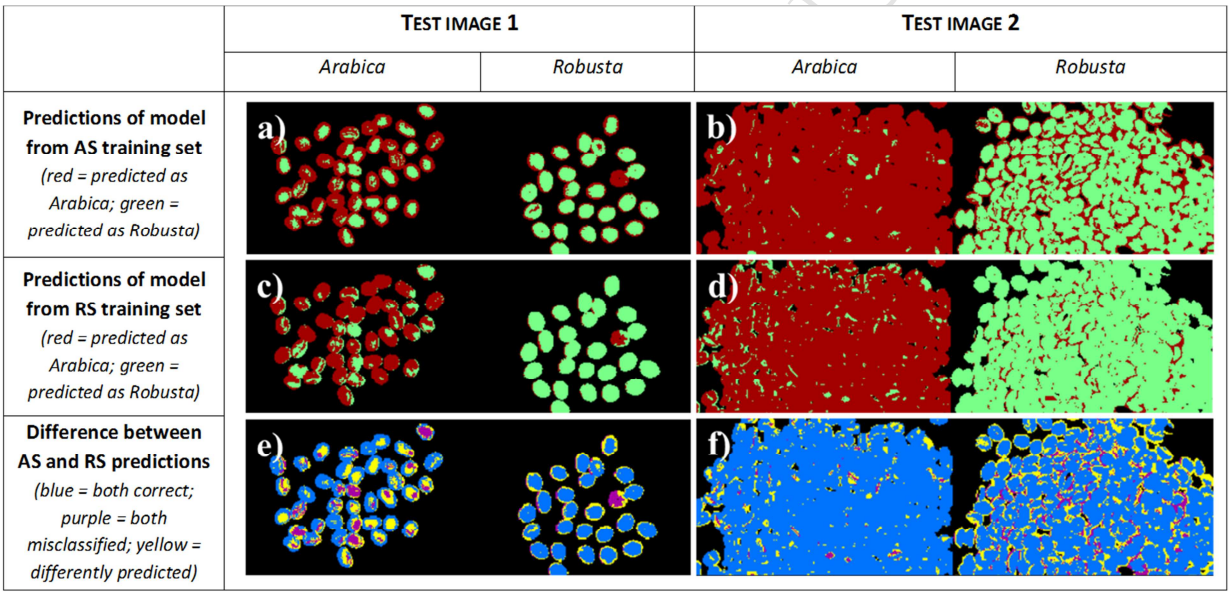


**Figure 4.** Filter simulation 3: predicted images of sPLS-DA models built using AS training set (a, b) and RS training set (c, d) and difference images for test image 1 (e) and test image 2 (f).

In order to better investigate the influence of shape-related effects, the Hotellig's $T^2$ values and the Q residuals of the sPLS-DA models discussed in this Section have also been considered. Actually, the pixels falling outside the 95% confidence limits are mainly placed at the edges of the beans, as reported in Figure S-7 of Supplementary material for the sPLS-DA model calculated with RS training set. In this case, only a small percentage of pixels was detected as outlier, thus the elimination of those pixels would have not significantly increased the classification performances.

However, it has to be highlighted that the implementation of outlier statistics in the classification model could be considered for a further optimization, giving the possibility to detect also potential foreign objects, such as metals, stones, sticks or soil residuals.

## 4 CONCLUSIONS

This paper is aimed at investigating the issues concerning the implementation of a multispectral imaging system, starting from the outcome of spectral feature selection performed using a hyperspectral system, in order to discriminate between Arabica and Robusta coffee species. In particular, the simulations reported in the present work were done not only considering the single reflectance values of the filters, but also exploring systematically linear and non-linear relationships between bands, and selecting the relevant descriptors involved in the classification, which led to a significant increase of the classification performances in prediction.

Moreover, attention was also paid to the proper construction of a representative training set by comparing two different approaches, which consisted in the use of average image spectra and of randomly selected spectra; the latter one led to better classification results, mostly in the case of predictions at the pixel-level, since it allowed to consider also the spatial variability within each image.

In the specific case, the use of a representative training set of randomly selected spectra allowed to better account for the round shape of the green coffee beans, while the selection of the most effective combinations of channels allowed to explore the descriptors which better reflect the chemical differences between Arabica and Robusta green coffee.

In particular, the proper combination of four NIR band-pass filters and the use of multivariate statistical analysis allowed to achieve classification performances comparable to those obtained with the hyperspectral data, i.e. considering the full NIR spectrum. Moreover, it has to be highlighted that the calculation of the 32 descriptors from the outputs of the band-pass filters and

the choice of the relevant ones involved in discrimination are conducted off-line during the optimization of the classification model. For the real-time implementation of the model only the four selected descriptors have to be calculated, which is much faster than acquiring and elaborating the whole spectrum (150 spectral variables) of the original hyperspectral imaging system. Based on these results, a filter-based multispectral imaging system can be easily implemented in order to obtain a fast and inexpensive tool suitable for on-line monitoring of green coffee, allowing to prevent counterfeits.

In general, the proposed approach demonstrated the possibility of having a clear idea of the classification performances that can be reached using a multispectral system, much time before the system itself is actually constructed.

## ACKNOWLEDGMENTS

The authors wish to thank Luigi Bellucci (Caffè Molinari S.p.A) for providing the coffee samples and technical support.

## REFERENCES

[1] D. Lorente, N. Aleixos, J. Gómez-Sanchis, S. Cubero, O.L. García-Navarrete, J. Blasco, Recent advances and applications of hyperspectral imaging for fruit and vegetable quality assessment. Food Bioprocess Tech. 5:4 (2012) 1121-1142.

[2] G. Elmasry, M. Kamruzzaman, D.W Sun, P. Allen, Principles and applications of hyperspectral imaging in quality evaluation of agro-food products: a review, CRC Cr. Rev. Food Sci. 52:11 (2012) 999-1023.

[3] A.A. Gowen, C. O'Donnell, P.J. Cullen, G. Downey, J.M. Frias, Hyperspectral imaging–an emerging process analytical tool for food quality and safety control. Trends Food Sci. Tech. 18:12 (2007) 590-598.

[4] J.M. Amigo, I. Martí, A. Gowen, A. Hyperspectral imaging and chemometrics: a perfect combination for the analysis of food structure, composition and quality. In: F. Marini (Ed), Data Handling in Science and Technology. Vol 28, 2013, pp. 343-370.

[5] C. Ferrari, G. Foca, A. Ulrici, Handling large datasets of hyperspectral images: reducing data size without loss of useful information, Anal. Chim. Acta 802 (2013) 29-39.

[6] C. Ferrari, G. Foca, R. Calvini, A. Ulrici, Fast exploration and classification of large hyperspectral image datasets for early bruise detection on apples, Chemometr. Intell. Lab. 146 (2015) 108-119.

[7] R. Calvini, A. Ulrici, J.M. Amigo, Practical comparison of sparse methods for classification of Arabica and Robusta coffee species using near infrared hyperspectral imaging, Chemometr. Intell. Lab. 146 (2015) 503-511.

[8] D. Lorente, N. Aleixos, J. Gomez-Sanchis, S. Cubero, O.L. Garcia-Navarrete, J. Blasco, Recent advances and applications of hyperspectral imaging for fruit and vegetable quality assessment, Food and Bioprocess Technology, 5:4 (2012) 1121-1142.

[9] P.M. Mehl, K. Chao, M. Kim, Y.R. Chen, Detection of defects on selected apple cultivars using hyper spectral and multispectral image analysis, Appl. Eng. Agric. 18:2 (2002) 219.

[10] W. Huang, J. Li, Q. Wang, L. Chen, Development of a multispectral imaging system for online detection of bruises on apples, J. Food Eng. 146 (2015) 62-71.

[11] O. Kleynen, V. Leemans, M.F. Destain, Development of a multi-spectral vision system for the detection of defects on apples, J. Food Eng. 69:1 (2005) 41-49.

[12] J. Qin, T.F. Burks, X. Zhao, N. Niphadkar, M.A. Ritenour, Development of a two-band spectral imaging system for real-time citrus canker detection. J. Food Eng. 108:1 (2012) 87-93.

[13] M.O. Ngadi, L. Liu, Hyperspectral image processing techniques, In: D.W. Sun (Ed.), Hyperspectral imaging for food quality analysis and control, 2010, pp 99-127.

[14] B. Park, K.C. Lawrence, W.R. Windham, D.P. Smith, Performance of hyperspectral imaging system for poultry surface fecal contaminant detection, J. Food Eng. 75:3 (2006) 340-348.

[15] M.J. Martín, F. Pablos, A.G. González, Discrimination between arabica and robusta green coffee varieties according to their chemical composition, Talanta 46:6 (1998) 1259-1264.

[16] F. Carrera, M. León-Camacho, F. Pablos, A.G. González, Authentication of green coffee varieties according to their sterolic profile, Anal. Chim. Acta 370:2 (1998) 131-139.

[17] C. Sanz, L. Maeztu, M.J. Zapelena, J. Bello, C. Cid, Profiles of volatile compounds and sensory analysis of three blends of coffee: influence of different proportions of Arabica and Robusta and influence of roasting coffee with sugar, J. Sci. Food Agr. 82:8 (2002) 840-847.

[18] R.C. Alves, S. Casal, M.R. Alves, M.B. Oliveira, Discrimination between arabica and robusta coffee species on the basis of their tocopherol profiles, Food Chem. 114 (2009) 295-299.

[19] R.M. El-Abassy, P. Donfack, A. Materny, Discrimination between Arabica and Robusta green coffee using visible micro Raman spectroscopy and chemometric analysis, Food Chem. 126:3 (2011) 1443-1448.

[20] R. Garrett, B.G. Vaz, A.M.C. Hovell, M.N. Eberlin, C.M. Rezende, Arabica and Robusta coffees identification of major polar compounds and quantification of blends by direct-infusion electrospray ionization-mass spectrometry. Journal of Agricultural and Food Chemistry, 60:17 (2012) 4253-4258.

[21] C. Martellossi, E.J. Taylor, D. Lee, G. Graziosi, P. Donini, DNA extraction and analysis from processed coffee beans, Journal of Agricultural and Food Chemistry, 53:22 (2005) 8432-8436.

[22] A.T. Toci, A. Farah, H.R. Pezza, L. Pezza, Coffee adulteration: More than two decades of research, Critical Reviews in Analytical Chemistry, 46:2 (2016) 83-92.

[23] Y.B. Monakhova, W. Ruge, T. Kuballa, M. Ilse, O. Winkelmann, B. Diehl, D.W. Lachenmeier, Rapid approach to identify the presence of Arabica and Robusta species in coffee using 1 H NMR spectroscopy, Food Chem. 182 (2015) 178-184.

[24] F. Wei, K. Furihata, M. Koda, F. Hu, R. Kato, T. Miyakawa, M. Tanokura, $^{13}$C NMR-based metabolomics for the classification of green coffee beans according to variety and origin, J. Agr. Food Chem. 60:40 (2012) 10118-10125.

[25] M. T. Gil-Agusti, N. Campostrini, L. Zolla, C. Ciambella, C. Invernizzi, P.G. Righetti, Two-dimensional mapping as a tool for classification of green coffee bean species, Proteomics 5:3 (2005) 710-718.

[26] S. Buratti, N. Sinelli, E. Bertone, A. Venturello, E. Casiraghi, F. Geobaldo, Discrimination between washed Arabica, natural Arabica and Robusta coffees by using near infrared spectroscopy, electronic nose and electronic tongue analysis, J. Sci. Food Agr. 95:11 (2015) 2192-2200.

[27] E.K. Kemsley, S. Ruault, R.H. Wilson, Discrimination between Coffea arabica and Coffea canephora variant robusta beans using infrared spectroscopy. Food Chem. 54:3 (1995) 321-326.

[28] J.R. Santos, M.C. Sarraguça, A.O. Rangel, J.A. Lopes, Evaluation of green coffee beans quality using near infrared spectroscopy: A quantitative approach. Food Chem. 135:3 (2012) 1828-1835.

[29] A.J. Myles, T.A. Zimmerman, S.D. Brown, Transfer of multivariate classification models between laboratory and process near-infrared spectrometers for the discrimination of green Arabica and Robusta coffee beans. App. Spectrosc. 60:10 (2006) 1198-1203.

[30] I. Esteban-Dıez, J.M. González-Sáiz, C. Pizarro, An evaluation of orthogonal signal correction methods for the characterisation of arabica and robusta coffee varieties by NIRS, Anal. Chim. Acta 514:1 (2004) 57-67.

[31] I. Esteban-Diez, J.M. González-Sáiz, C. Sáenz-González, C. Pizarro, Coffee varietal differentiation based on near infrared spectroscopy, Talanta, 71:1 (2007) 221-229.

[32] A.G. Fiore, R. Romaniello, G. Peri, C. Severini, Quality assessment of roasted coffee blends by hyperspectral image analysis. In Proceedings of 22nd International Conference on Coffee Science, Campinas, Brazil, 2008.

[33] A. Backhaus, F. Bollenbeck, U. Seiffert, High-throughput quality control of coffee varieties and blends by artificial neural networks and hyperspectral imaging. In Proceedings of the 1st International Congress on Cocoa, Coffee and Tea, CoCoTea, 2011.

[34] S. Chevallier, D. Bertrand, A. Kohler, P. Courcoux, Application of PLS-DA in multivariate image analysis, J. Chemometr. 20:5 (2006) 221.

[35] M.A.F. de la Ossa, C. García-Ruiz, J.M. Amigo, Near infrared spectral imaging for the analysis of dynamite residues on human handprints, Talanta, 130 (2014) 315-321.

[36] K.A. Lê Cao, S. Boitard, P. Besse, Sparse PLS discriminant analysis: biologically relevant feature selection and graphical displays for multiclass problems, BMC bioinformatics, 12(1) (2011) 253.

[37] J. Burger, P. Geladi, Hyperspectral NIR image regression part II: dataset preprocessing diagnostics, J. Chemometr. 20:3 (2006) 106-119.

[38] J. Burger, P. Geladi, Hyperspectral NIR image regression part I: calibration and correction, J. chemometr. 19:5 (2005) 355-363.

[39] A. Ulrici, S. Serranti, C. Ferrari, D. Cesare, G. Foca, G. Bonifazi, Efficient chemometric strategies for PET–PLA discrimination in recycling plants using hyperspectral imaging, Chemometr. Intell. Lab., 122 (2013) 31-39.

[40] P. Filzmoser, M. Gschwandtner, V. Todorov, Review of sparse methods in regression and classification with application to chemometrics, J. Chemometr. 26 (2012) 42-51.

[41] M.A. Rasmussen, R. Bro, A tutorial on the Lasso approach to sparse modelling, Chemometr. Intell. Lab. 119 (2012) 21-31.

[42] T.M. Cover, P.E. Hart, Nearest neighbour pattern classification, IEEE T. Inform. Theory, 13:1 (1967) 21-27.

[43] J.S. Shenk, J.J. Workman, M.O. Westerhaus, Application of NIR spectroscopy to agricultural products. In D.A. Burns, E.W. Ciurczak (Eds.), Handbook of Near Infrared Analysis, Third Edition, Boca Raton: CRC Press, 2008, pp. 347-386.

[44] NIR Bandpass & Laser Line Filters: 700 - 1650 nm Center Wavelength. URL http://www.thorlabs.de/newgrouppage9.cfm?objectgroup_id=1000 . Accessed 19.08.15.

[45] M. Calderisi, A. Ulrici, S. Sinisalo, J. Uotila, R. Seeber, Simulation of an experimental database of infrared spectra of complex gaseous mixtures for detecting specific substances. The case of drug precursors. Sensor. Actuat. B: Chem. 193 (2014) 806-814.

[46] N.F. Pérez, J. Ferré, R. Boqué, Calculation of the reliability of classification in discriminant partial least-squares binary classification, Chemometr. Intell. Lab. 95:2 (2009) 122-128.

[47] E. Szymanska, E. Brodrick, M. Williams, A.N. Davies, H.J. Van Manen, L.C.M Buydens, Data size reduction strategy for the classification of breath and air samples using multicapillary column-ion mobility spectrometry, Analytical Chemistry 87:2 (2015) 869-875.

## CAPTURES TO FIGURES

**Figure 1.** Average spectra calculated from each image of the training samples with selected regions highlighted (a), Gaussian profiles of the 4 filters considered (b) and resulting reflectance values obtained from the average training spectra (c).

**Figure 2.** Filter simulation 1: predicted images of PLS-DA models built using AS training set (a, b) and RS training set (c, d), and difference images for test image 1 (e) and test image 2 (f).

**Figure 3.** PLS-DA regression vectors of the classification models built on AS training set (a) and RS training set (b) considered in filter simulation 2; and regression vectors of sPLS-DA models calculated on AS training set (a) and RS training set (b) in filter simulation 3.

**Figure 4.** Filter simulation 3: predicted images of sPLS-DA models built using AS training set (a, b) and RS training set (c, d) and difference images for test image 1 (e) and test image 2 (f).

**Table 1.** List of the 32 descriptors considered.

| Single Filters | Differences | Ratios | Products | Sums |
|---|---|---|---|---|
| R1150 | R1200-R1150 | R1150/R1200 | R1150*R1200 | R1150+R1200 |
| R1200 | R1250-R1200 | R1150/R1250 | R1150*R1250 | R1150+R1250 |
| R1250 | R1400-R1250 | R1150/R1400 | R1150*R1400 | R1150*R1400 |
| R1400 | R1400-R1200 | R1200/R1250 | R1200*R1250 | R1200+R1250 |
| $R1150^2$ | R1400-R1150 | R1200/R1400 | R1200*R1400 | R1200+R1400 |
| $R1200^2$ | R1250-R1150 | R1250/R1400 | R1250*R1400 | R1250+R1400 |
| $R1250^2$ | | | | |
| $R1400^2$ | | | | |

**Table 2.** Results obtained using AS training set and RS training set in filters simulation1, filter simulation 2 and filter simulation 3; the classification efficiency values are referred to the results in calibration ($EFF_{CAL}$), cross-validation ($EFF_{CV}$), prediction of the test set at the image-level ($EFF_{TEST}$), and of test image 1 and test image 2 at the pixel-level ($EFF_{IMG1}$ and $EFF_{IMG2}$, respectively).

| | **Filter Simulation 1** | | **Filter Simulation 2** | | **Filter Simulation 3** | |
|---|---|---|---|---|---|---|
| | **AS tr. set** | **RS tr. set** | **AS tr. set** | **RS tr. set** | **AS tr. set** | **RS tr. set** |
| **N° variables** | 4 | 4 | 32 | 32 | 4 | 4 |
| **LVs** | 4 | 4 | 3 | 3 | 2 | 2 |
| $\boldsymbol{EFF_{CAL}}$ | 99.1 | 81.3 | 100.0 | 80.3 | 99.6 | 78.4 |
| $\boldsymbol{EFF_{CV}}$ | 97.3 | 79.9 | 99.3 | 78.7 | 97.3 | 78.0 |
| $\boldsymbol{EFF_{TEST}}$ | 94.0 | 94.9 | 97.5 | 100.0 | 98.3 | 100.0 |
| $\boldsymbol{EFF_{IMG1}}$ | 65.1 | 74.0 | 71.1 | 71.0 | 69.5 | 83.9 |
| $\boldsymbol{EFF_{IMG2}}$ | 83.9 | 92.2 | 84.3 | 92.1 | 85.6 | 93.1 |

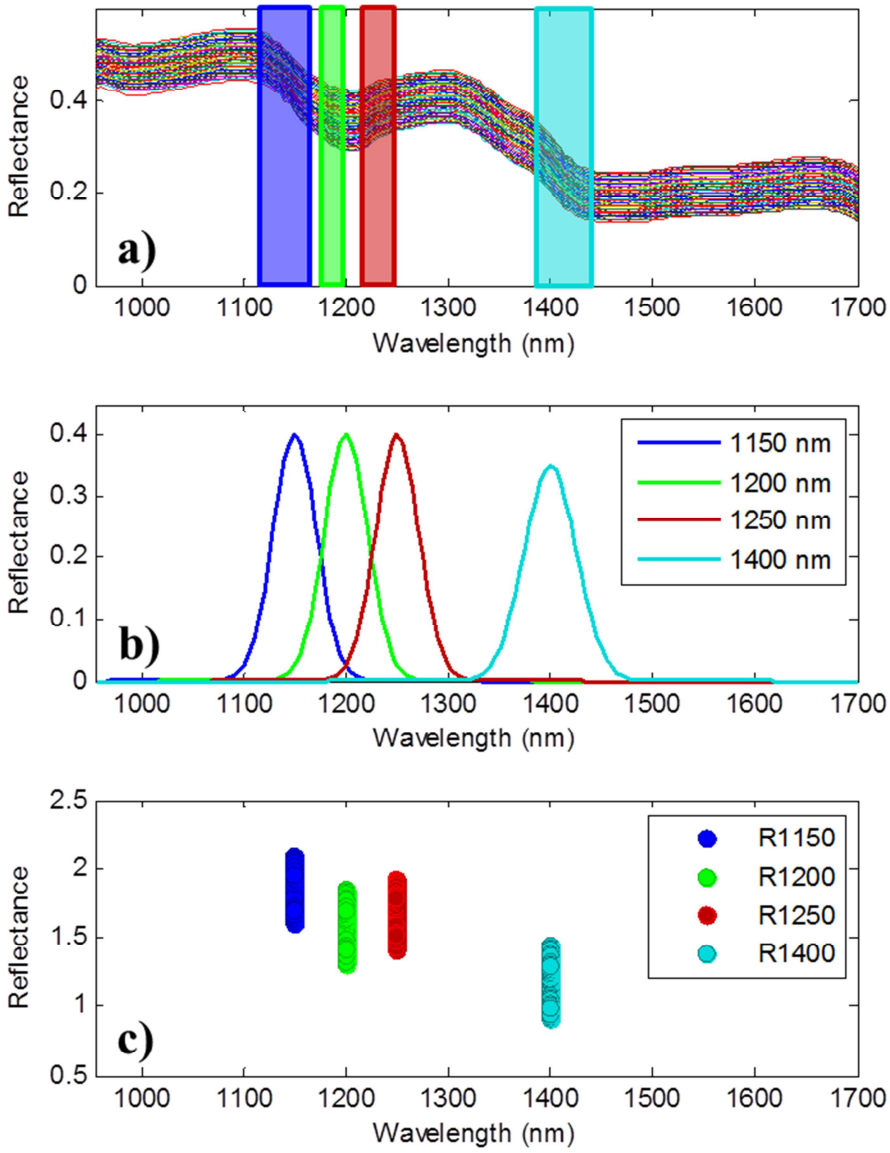

| | TEST IMAGE 1 | | TEST IMAGE 2 | |
|---|---|---|---|---|
| | *Arabica* | *Robusta* | *Arabica* | *Robusta* |
| **Predictions of model from AS training set** *(red = predicted as Arabica; green = predicted as Robusta)* | a) | | b) | |
| **Predictions of model from RS training set** *(red = predicted as Arabica; green = predicted as Robusta)* | c) | | d) | |
| **Difference between AS and RS predictions** *(blue = both correct; purple = both misclassified; yellow = differently predicted)* | e) | | f) | |

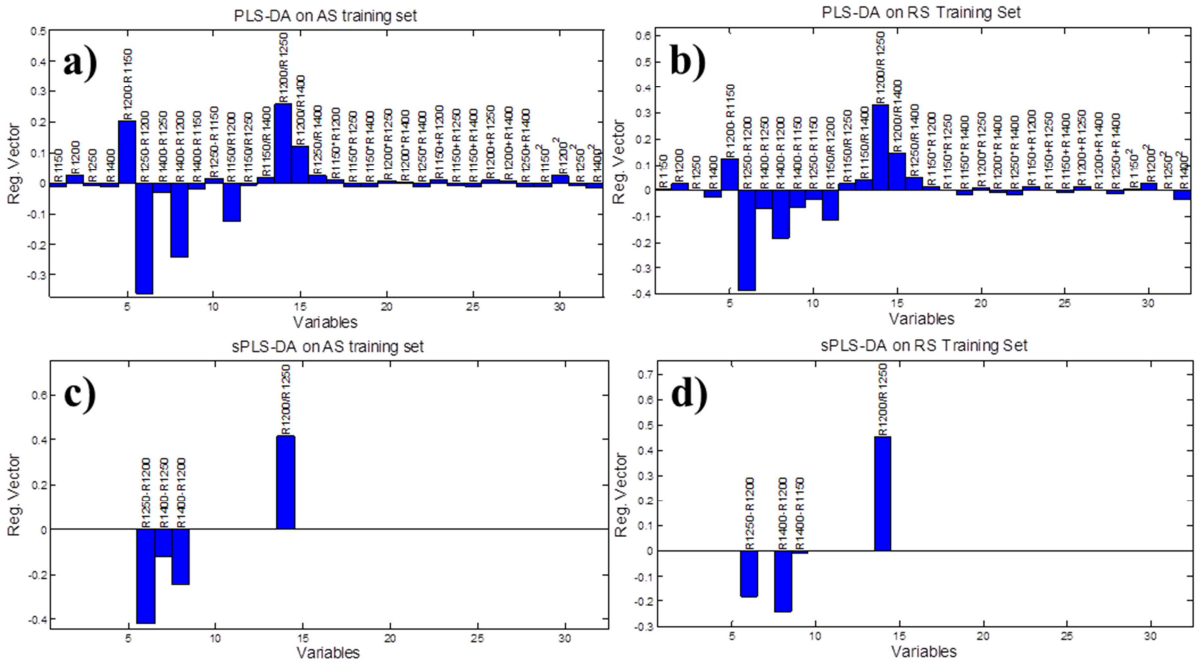

| | TEST IMAGE 1 | | TEST IMAGE 2 | |
|---|---|---|---|---|
| | *Arabica* | *Robusta* | *Arabica* | *Robusta* |
| **Predictions of model from AS training set** *(red = predicted as Arabica; green = predicted as Robusta)* | 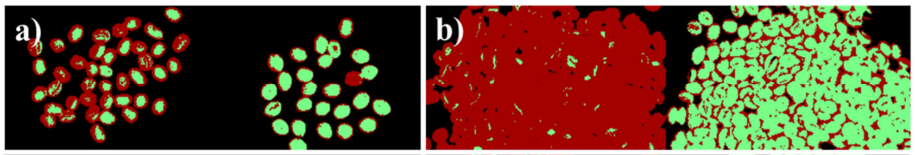  | | | |
| **Predictions of model from RS training set** *(red = predicted as Arabica; green = predicted as Robusta)* | 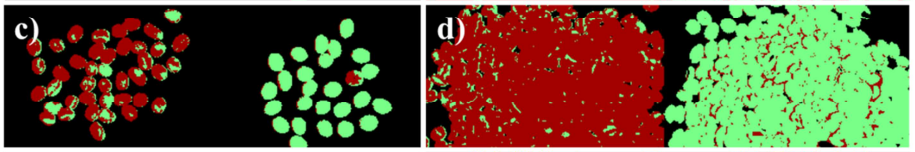  | | | |
| **Difference between AS and RS predictions** *(blue = both correct; purple = both misclassified; yellow = differently predicted)* | 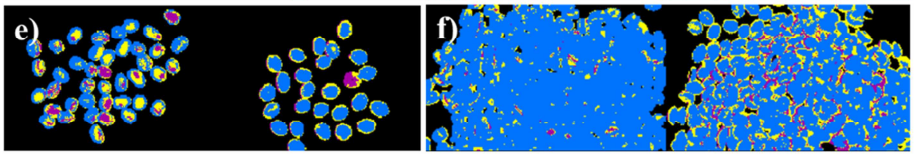  | | | |

**Highlights**

- Fast discrimination between Arabica and Robusta is important for coffee industry
- Multispectral imaging can be very effective to this aim, but hard to implement
- Multispectral data were simulated from HSI data and NIR band-pass filters
- sPLS-DA was used for classification and selection of the relevant descriptors
- Classification performances were evaluated both at image-level and at pixel-level